UDC 519.63

COMPARISON OF FINITE DIFFERENCE AND FINITE VOLUME METHODS FOR NUMERICAL SIMULATION OF FILTRATION IN A CYLINDRICAL POROUS FILTER

[1*]***Berdiyorov Sh.Sh.,*** [2]***Ermonova M.U.***

[*]berdiyorovsh@gmail.com

[1]Digital Technologies and Artificial Intelligence Development Research Institute,
17A, Buz-2, Tashkent, 100125 Uzbekistan;

[2]Gulistan State Pedagogical Institute,
49, Talabalar Street, Gulistan, 120105 Uzbekistan

This study presents a comparative numerical investigation of the Finite Difference Method (FDM) and the Finite Volume Method (FVM) for simulating filtration processes in a cylindrical porous filter. The mathematical model combines axisymmetric Brinkman–Darcy flow equations with advection–diffusion–reaction equations describing the transport of dissolved substances in a porous medium. Both numerical methods are applied to the same mathematical model under identical initial, boundary, and computational conditions. The comparison considers pressure and velocity distributions, solute concentration, numerical accuracy, grid convergence, conservation properties, stability, and computational efficiency. Numerical experiments are performed to evaluate the influence of the computational method on the simulation results. The results demonstrate the advantages and differences of the finite difference and finite volume approaches and provide a basis for selecting an appropriate numerical method for modeling filtration processes in cylindrical porous media.

Keywords: cylindrical porous filter, filtration processes, Brinkman–Darcy model, finite difference method, finite volume method, numerical simulation

Citation: Berdiyorov Sh.Sh., Ermonova M.U. 2026. Comparison of finite difference and finite volume methods for numerical simulation of filtration in a cylindrical porous filter. *Problems of Computational and Applied Mathematics.* 4(74): 65-84.

DOI: 10.71310/pcam.4_74.2026.04

1 Introduction

Filtration and transport processes in porous media play an important role in many industrial, environmental, and technological applications, including water treatment, chemical separation, membrane filtration, and purification systems. The efficiency of these processes depends on the properties of the porous medium, flow conditions, and transport mechanisms occurring inside the filter. In cylindrical porous filters, the interaction between fluid flow and mass transport leads to complex distributions of pressure, velocity, and concentration.

Mathematical modeling provides an effective approach for investigating these processes and predicting the behavior of porous filtration systems. The filtration flow can be described using the Brinkman–Darcy equations, while the transport of dissolved substances is commonly represented by advection–diffusion–reaction equations. The numerical solution of these coupled equations requires the selection of an appropriate computational method capable of providing accurate and stable results.

Among the numerical approaches used for solving filtration and transport problems, the Finite Difference Method (FDM) and the Finite Volume Method (FVM) are widely

applied. The finite difference approach approximates the differential equations directly at discrete grid points and provides a relatively simple computational implementation. The finite volume approach is based on the integration of governing equations over control volumes and provides a conservative formulation of the transport and flow processes. Previous studies have investigated filtration and transport processes in cylindrical porous media using finite difference and finite volume approaches separately. However, the numerical characteristics of these methods may differ depending on the computational grid, discretization procedure, and conservation properties. Therefore, a direct comparison under identical mathematical and computational conditions is necessary to evaluate their applicability to cylindrical porous filtration problems.

The aim of this study is to compare the Finite Difference Method and the Finite Volume Method for the numerical simulation of filtration in a cylindrical porous filter. Both methods are applied to the same mathematical model based on the axisymmetric Brinkman–Darcy equations and transport equations under identical initial and boundary conditions. The obtained numerical results are compared in terms of pressure and velocity distributions, concentration fields, numerical accuracy, stability, conservation properties, grid convergence, and computational efficiency. The results of the study provide a basis for evaluating the advantages and limitations of both methods and selecting an appropriate numerical approach for modeling filtration and transport processes in cylindrical porous media.

The study [1] develops a mathematical and computational model for describing filtration flow, solute transport, adsorption, and membrane fouling in a cylindrical porous filter. The model integrates axisymmetric Brinkman–Darcy equations with advection–diffusion–reaction processes, Langmuir adsorption, and linear driving force (LDF) kinetics. Changes in porosity, particle deposition, cake-layer formation, osmotic pressure, and increasing membrane resistance are also incorporated. Numerical simulations are performed using a finite difference scheme with CFL-based stability control. The results indicate that adsorption and particle accumulation decrease the porosity and permeability of the filter, resulting in higher hydraulic resistance and a gradual reduction in filtration flux. The developed model can be used to analyze fouling behavior and support the optimization of porous filtration systems.

A mathematical and computational model for the filtration of liquid solutions in a cylindrical porous filter was proposed in [2]. The model is based on the Brinkman–Darcy equations to describe fluid flow through the porous medium, while the relationship between porosity and permeability is determined using the Kozeny–Carman equation. The transport of dissolved substances is described by an advection–diffusion–reaction model coupled with the linear driving force (LDF) kinetic approach and the Langmuir adsorption isotherm. In addition, particle deposition and colmatation are considered, resulting in a gradual reduction of filter porosity over time. The numerical solution is obtained using a finite difference scheme based on a combined gradient approach with an iterative pressure-correction procedure, while numerical stability is controlled according to the Courant–Friedrichs–Lewy condition.

The study [3] investigates the numerical modeling of filtration flow and dissolved component transport in a cylindrical porous medium. The mathematical model is based on the axisymmetric Brinkman–Darcy equations for describing fluid motion and a system of convection–diffusion–adsorption equations for mass transport in the porous structure. The numerical solution is obtained using the Finite Volume Method, which ensures the conservation of governing quantities within each control volume. A computational algo-

rithm is developed to determine the pressure distribution, velocity field, and concentration of dissolved components. The study also analyzes the influence of the porous structure on the adsorption kinetics and the overall characteristics of the filtration process.

Work [4] presents an analytical solution to a filtration problem in a sandwich-type collector system, with particular attention given to determining the pressure distribution within a low-permeability layer. The study also proposes a generalized approach for the management of well galleries. The developed mathematical framework can be applied to the design and evaluation of vertical drainage well systems, flood prevention in irrigated and non-irrigated areas, groundwater protection from pollution, and the development of strategies for isolating contaminated zones.

In work [5], a mathematical model and an efficient numerical algorithm were developed to investigate the technological processes involved in the filtration of liquid and ionized solutions. The model considers variations in filtration rate and suspension concentration within the filter column and at the outlet, as well as the formation of a sediment layer on the filter surface and the accumulation of gel particles inside the pores. Changes in pressure within both the filtration column and the sediment layer, together with other physical and mechanical properties of the filtered liquid, are also taken into account. Computational experiments were performed, and the results were presented graphically to examine the operating behavior of the filtration system under different suspension characteristics and external conditions.

Study [6] presents a numerical approach for the simultaneous simulation of seepage flow in porous media and Navier–Stokes flow in a pure fluid region. The method is based on the Darcy–Brinkman equations, which provide a continuous representation of the flow velocity across the interface between the porous and fluid domains. Spatial discretization is performed using the Finite Volume Method, while a fractional-step approach is applied to simulate incompressible fluid flow. The coupling between the two flow regions is achieved by interpolating pressure and velocity at the interface, where permeability and porosity exhibit discontinuities. The proposed interpolation schemes improve numerical stability and eliminate the need to explicitly resolve the thin transition zone near the interface. Numerical tests involving one-dimensional uniform flow, lid-driven cavity flow, and pipe flow in porous media demonstrated that the method provides stable, accurate, and physically realistic results.

Work [7] investigates a hybrid-dimensional model of compressible fluid flow in fractured porous media from both theoretical and numerical perspectives. The flow is described by the Brinkman model within the fracture and the Darcy model in the surrounding porous medium. A finite volume scheme with a minimal number of nodal points is developed to solve the coupled model on non-matching computational grids. Second-order error estimates for pressure and velocity are derived with respect to different mesh sizes. Numerical experiments confirm the accuracy and efficiency of the proposed approach, while additional simulations examine the effects of permeability, fracture width, effective viscosity, and other model parameters on fluid flow behavior in the fractured porous system.

The study [8] addresses the numerical simulation of single-phase flow coupled with reactive transport in porous media, which involves solving a highly nonlinear system of coupled differential equations. A fully implicit Finite Volume Method based on a direct substitution approach is proposed to improve the accuracy and efficiency of the numerical solution. The method is implemented within the parallel open-source DuMuX platform and can handle different coupling strategies for reactive transport problems. Several two- and three-dimensional numerical experiments are conducted to evaluate the

performance of the proposed approach, including benchmark problems and simulations of long-term CO_2 storage. The results also compare the direct substitution and sequential iterative approaches and investigate the parallel scalability of the method for different computational grid resolutions.

Study [9] proposes a high-order numerical method for solving the two-dimensional semilinear compressible Darcy–Brinkman equation in porous media. The spatial discretization combines block-centered and compact finite difference techniques, while time integration is performed using an implicit–explicit fourth-order backward differentiation formula (IMEX-BDF4). The stability and error properties of the scheme are theoretically analyzed for both the solution and flux. Numerical experiments demonstrate fourth-order convergence in space and time, confirming the high accuracy and computational efficiency of the proposed method.

Work [10] investigates a coupled slightly compressible Darcy–Brinkman flow and transport problem in fractured porous media at relatively high Reynolds numbers. The model describes Brinkman flow within fractures coupled with advection–diffusion transport throughout the porous medium. A reduced two-layer model is introduced by representing the fracture as a lower-dimensional interface. The resulting system is solved using a finite difference method with a second-order backward differentiation scheme and a modified upwind discretization on staggered nonuniform grids. The theoretical analysis establishes the existence and uniqueness of the solution and demonstrates second-order convergence under mass-conservative transmission and Beavers–Joseph–Saffman interface conditions. Numerical experiments confirm the accuracy and efficiency of the method and illustrate fluid flow and solute transport in porous media containing intersected, embedded, and L-shaped fractures.

Study [11] presents a coupled model for simulating Brinkman flow and reactive transport in fractured porous media. The Brinkman equation is used to describe fluid flow within fractures, accounting for porous resistance and viscous shear effects at the fracture walls. The model is coupled with advection–diffusion–reaction transport and includes the evolution of porosity, fracture aperture, and precipitation concentration caused by chemical reactions. A space–time algorithm based on the Finite Volume Method is developed to solve the resulting hybrid-dimensional coupled system. The algorithm sequentially decouples the governing ODEs and PDEs at each time step and can effectively handle discontinuities in pressure, concentration, and reaction terms. Theoretical error analysis demonstrates second-order accuracy in both space and time, while numerical experiments confirm the accuracy and efficiency of the proposed method for porous media with variable fractures.

Study [12] investigates the application of a cell-centered Finite Volume Method for coupled hydromechanical processes in porous media. The proposed approach provides a compatible finite volume discretization for both fluid flow and mechanical deformation, avoiding the need for separate computational grids or mixed finite-volume–finite-element formulations. Particular attention is given to the treatment of coupling terms between flow and deformation. The method also allows fractured and heterogeneous porous media to be represented through internal boundary conditions. Numerical examples are used to examine the convergence properties of the coupled scheme and to demonstrate its applicability to fractured and heterogeneous porous media.

Work [13] presents a systematic comparison of the Stokes–Brinkman and Darcy–Darcy models for simulating steady-state creeping flow in fractured porous media. The two approaches are evaluated in terms of numerical accuracy and computational efficiency.

Sensitivity analyses are performed to investigate the effects of fracture orientation and size, mesh resolution, and local grid refinement. The accuracy of the numerical solutions is assessed using the R2 coefficient and the L2 norm. The results show that both models produce similar pressure and velocity fields under certain flow conditions, while their computational performance and sensitivity to mesh resolution differ. The Stokes–Brinkman model is found to be more sensitive to mesh resolution, whereas local grid refinement improves its accuracy on coarse meshes. The study provides a useful methodological basis for comparing numerical models according to accuracy, mesh convergence, and computational efficiency.

Study [14] examines how different numerical formulations of governing partial differential equations can affect the accuracy of simulations for unsaturated flow in porous media. The results show that the standard head-based form of the Richards equation may produce significant mass-balance errors and inaccurate predictions of infiltration depth. In contrast, the mixed formulation provides better mass conservation and improves the overall numerical solution without additional computational cost. The study also emphasizes the importance of properly discretizing the time derivative, demonstrating that the use of a diagonal time matrix helps satisfy the maximum principle and produces smooth, nonoscillatory infiltration profiles. These findings highlight the importance of conservation properties and numerical discretization in obtaining accurate solutions for flow problems in porous media.

Work [15] provides a fundamental theoretical framework for understanding groundwater flow and contaminant transport in porous media. It discusses key processes such as Darcy flow, mass conservation, advection, diffusion, and dispersion, together with mathematical formulations and numerical approaches for their analysis. The book therefore serves as an important theoretical reference for studying filtration and solute transport in porous media and for developing numerical models using the Finite Difference and Finite Volume Methods.

2 Problem formulation

Below are the equations for a cylindrical porous filter.

Equations for hydraulics (Brinkman–Darcy):

$$\frac{1}{r}\frac{\partial(ru_r)}{\partial r} + \frac{\partial u_z}{\partial z} = 0, \tag{1}$$

$$-\frac{\mu}{\varkappa(\varepsilon)}u_r + \mu\left(\frac{1}{r}\frac{\partial}{\partial r}\left(r\frac{\partial u_r}{\partial r}\right) + \frac{\partial^2 u_r}{\partial z^2} - \frac{u_r}{r^2}\right) - \frac{\partial p}{\partial r} = 0, \tag{2}$$

$$-\frac{\mu}{\varkappa(\varepsilon)}u_z + \mu\left(\frac{1}{r}\frac{\partial}{\partial r}\left(r\frac{\partial u_z}{\partial r}\right) + \frac{\partial^2 u_z}{\partial z^2}\right) - \frac{\partial p}{\partial z} = 0, \tag{3}$$

$$\varkappa(\varepsilon) = \frac{\varepsilon^3 d_f^2}{180(1-\varepsilon)^2}. \tag{4}$$

Here: r is the radial coordinate $[m]$, z is the vertical coordinate $[m]$, u_r is the radial velocity component $[m/s]$, u_z is the vertical velocity component $[m/s]$, the angular coordinate is taken as zero due to symmetry, $\mu = \mu(T)$ denotes the dynamic viscosity $[Pa{\cdot}s]$, $\varkappa(\varepsilon)$ is the permeability $[m^2]$, p is the pressure $[Pa]$, ε is the porosity, $(0 < \varepsilon < 1)$, d_f is the filter particle diameter $[m]$.

Here, (1) is the conservation of mass equation and represents the uncompressibility of water. It ensures the balance of incoming and outgoing volumes, ensuring mass preservation regardless of the internal pressure in the filter. Equation (2) corresponds to the radial balance of momentum, which describes the radial velocity under the influence of the pressure gradient and the resistance of the porous medium. When there is a pressure difference between the center and the wall, the fluid moves radially, and the resistance of the pores slows down this movement. The next equation controls the axial pulse, which controls the flow in the main direction from top to bottom. Here, the pressure difference drives the motion, while the viscosity and porosity resistance reduce the flow rate. As a result, the flow rate depends on the applied pressure gradient. The last equation is the Kozeny–Carman relation, which relates the internal structure of the filter, in particular its porosity, to its permeability. A more porous or coarse-grained medium allows fluid to pass through more easily and increases overall permeability.

For liquids, the viscosity is approximated as

$$\mu = a \cdot 10^{\frac{b}{T-c}}. \tag{5}$$

Where again T is absolute temperature and a, b and c are experimentally determined constants.

For substance transport (for each $i = 1, \ldots, N$), the following equations (6)–(9) are expressed:

$$\frac{\partial(\varepsilon c_i)}{\partial t} + \nabla \cdot (u c_i) = \nabla \cdot (\varepsilon D_i \nabla c_i) - r_i^{\text{bulk}} - a_s r_i^{\text{surf}}, \tag{6}$$

$$\frac{\partial q_i}{\partial t} = k_{f,i}(q_i^* - q_i), \tag{7}$$

$$q_i^* = \frac{q_{i,\max} b_i c_i}{1 + \sum_{j=1}^{N} b_j c_j}, \tag{8}$$

$$r_{i,\text{surf}} = \rho_s \frac{\partial q_i}{\partial t}. \tag{9}$$

where t is time $[s]$, N is the number of components, c_i – concentration of the i-th component in water $[mol/m^3$ or $kg/m^3]$, $D_{i,\text{eff}}$ – effective diffusion coefficient $[m^2/s]$, $r_{i,\text{bulk}}$ – bulk reaction rate in solution $[mol/(m^3 \cdot s)]$, a_s – surface area per unit volume $[m^2/m^3]$, $r_{i,\text{surf}}$ – surface loss rate $[mol/(m^2 \cdot s)]$, q_i – capture quantity in the solid phase $[mol/kg]$, $k_{f,i}$ – LDF(linear driving force) kinetic coefficient $[1/s]$, q_i^* – equilibrium adsorption quantity $[mol/kg]$, $q_{i,\max}$ – maximum adsorption capacity $[mol/kg]$, b_i – Langmuir affinity coefficient $[m^3/mol]$, ρ_s – density of adsorbent particles $[kg/m^3]$.

Equation (6) is the advection–diffusion–reaction (ADR) equation, which describes how the concentration of each pollutant in the water changes. It accounts for changes due to transport by flow (advection), dispersion by diffusion, elimination by reaction, and reduction by adsorption. This equation is used to evaluate the quality of filtered water at the outlet. Equation (7) represents a linear kinetic model of adsorption, which determines the rate of contaminant retention by filter particles. With a large number of adsorption sites, absorption is fast, but as the particles become saturated, the adsorption rate decreases. The next equation is the Langmuir isotherm, which describes the adsorption state under limited surface conditions. Due to limited adsorption sites, pollutants compete for free space, and filtration efficiency gradually decreases over time. The latter equation

describes the rate of change of the surface load, shows how adsorption in the solid phase develops and reduces the concentration in the liquid phase. This term relates the transfer of pollutants between the liquid and solid phases through the process of adsorption.

The colmatation equations (10)–(11) are defined as follows:

$$\frac{\partial(\varepsilon c_p)}{\partial t} + \frac{1}{r}\frac{\partial}{\partial r}(r c_p u_r) + \frac{\partial}{\partial z}(c_p u_z) = \frac{1}{r}\frac{\partial}{\partial r}\left(r\varepsilon D_p \frac{\partial c_p}{\partial r}\right) + \frac{\partial}{\partial z}\left(\varepsilon D_p \frac{\partial c_p}{\partial z}\right) - k_{\text{dep}} c_p, \quad (10)$$

$$\frac{\partial \varepsilon}{\partial t} = -\frac{\nu_{\text{dep}}}{\rho_{\text{dep}}} k_{\text{dep}} c_p. \quad (11)$$

where c_p – concentration of particulate matter in water [kg/m^3], D_p – diffusion coefficient of particles [m^2/s], k_{dep} – deposition coefficient [1/s], ν_{dep} – volume fraction of deposition [–], ρ_{dep} – density of settled particles [kg/m^3].

In this situation, larger particles such as sand and clay clog the pores, leading to a reduction in the filter's permeability. Consequently, the flow rate gradually decreases over time.

$$J_i = (1 - \sigma_i)\, c_{i,\text{avg}}\, J_v - P_{s,i}\, \Delta c_i, \quad (12)$$

$$J_v = \frac{\Delta p}{\mu(R_m + R_c)}, \quad (13)$$

$$R_c = \alpha_c \delta_c, \quad (14)$$

$$\frac{\partial \delta_c}{\partial t} = \frac{J_v\, c_{p,m}}{\rho_c}. \quad (15)$$

Here: G_{in} – inlet surface (from above, $z = 0$), G_{out} – outlet surface (from below, $z = H$), J_v – volumetric flow through the membrane (permeat flux) $[m/\text{s}]$, L_p – membrane hydraulic permeability $[m/(Pa{\cdot}s)]$, Δp – transmembrane pressure difference $[Pa]$, σ_i – reflection coefficient [-], π_i – osmotic pressure $[Pa]$, J_i – membrane flow of the i-th component $[mol/(m^2{\cdot}s)]$, $c_{i,\text{avg}}$ – average concentration near the membrane $[mol/m^3]$, $P_{s,i}$ – salt permeability $[m/s]$, $\partial/\partial n$ – normal derivative operator (at the membrane level), R_m – internal membrane resistance $[1/m]$, R_c – cake resistance $[1/m]$, α_c – specific cake resistance $[m/kg]$, $\delta_c(r, z, t)$ – cake thickness $[m]$, $c_{p,m}$ – particle concentration on the membrane $[kg/m^3]$, ρ_c – cake density $[kg/m^3]$.

2.1 Boundary and initial conditions

The computational domain is an axisymmetric cylindrical domain

$$\Omega = \{(r, z) : 0 \leqslant r \leqslant R,\ 0 \leqslant z \leqslant H\}. \quad (16)$$

To close the system of equations (1)–(8), the following boundary and initial conditions are specified.

At the filter inlet ($z = 0$), a uniform axial flow of liquid and known concentrations of components are set:

$$\begin{cases} u_z(r, 0) = u_{in}, \\ u_r(r, 0) = 0, \\ c_i(r, 0) = c_{i,in},\ i = 1, \ldots, N. \end{cases} \quad (17)$$

Neumann's condition is used for pressure:

$$\left.\frac{\partial p}{\partial z}\right|_{z=0} = 0. \tag{18}$$

At the filter outlet ($z = H$), a fixed pressure is set, and for the remaining values, the conditions of zero longitudinal gradient are met:

$$\begin{cases} p\left(r, H\right) = p_{out}, \\ \left.\dfrac{\partial u_z}{\partial z}\right|_{z=H} = J_v, \\ \left.\dfrac{\partial u_r}{\partial z}\right|_{z=H} = 0, \\ \left.\dfrac{\partial c_i}{\partial z}\right|_{z=H} = 0, \ i = 1, \ldots, N. \end{cases} \tag{19}$$

Axis of symmetry ($r = 0$): Due to the axisymmetric nature of the solution, the following conditions are satisfied:

$$\begin{cases} u_r\left(0, z\right) = 0, \\ \left.\dfrac{\partial u_z}{\partial r}\right|_{r=0} = 0, \\ \left.\dfrac{\partial p}{\partial r}\right|_{r=0} = 0, \\ \left.\dfrac{\partial c_i}{\partial r}\right|_{r=0} = 0, \ i = 1, \ldots, N. \end{cases} \tag{20}$$

Side surface of the filter ($r = R$): On the side wall of the filter, the adhesion conditions for the velocity and the absence of diffusion flow of substances are set:

$$\begin{cases} u_r\left(R, z\right) = 0, \\ u_z\left(R, z\right) = 0, \\ \left.\dfrac{\partial p}{\partial r}\right|_{r=R} = 0, \\ \left.\dfrac{\partial c_i}{\partial r}\right|_{r=R} = 0, \ \ i = 1, \ldots, N. \end{cases} \tag{21}$$

Membrane level (if applicable, G_m) boundary conditions

$$\begin{cases} u_n = J_v, \quad J_v = L_p\left(\Delta p - \sum\limits_{i=1}^{N} \sigma_i \Delta \pi_i\right), \\ J_v = \dfrac{\Delta p}{\mu\left(R_m + R_c\right)}, \\ -\varepsilon D_{i,\text{eff}} \dfrac{\partial c_i}{\partial n} + u_n c_i = J_i, \quad i = 1, \ldots, N, \\ J_i = \left(1 - \sigma_i\right) J_v c_{i,\text{avg}} - P_{s,i} \Delta c_i. \end{cases} \tag{22}$$

Initial conditions ($t = 0$). For a non-stationary problem, the initial conditions are given in the form:

$$u_r\left(r, z, 0\right) = u_{r,0}\left(r, z\right), \ u_z\left(r, z, 0\right) = u_{z,0}\left(r, z\right), \ p\left(r, z, 0\right) = p_0\left(r, z\right), \tag{23}$$

$$\begin{cases} c_i(r,z,0) = c_{i,0}, \\ q_i(r,z,0) = 0, \quad i = 1, \ldots, N, \\ \varepsilon(r,z,0) = \varepsilon_0(r,z), \quad \delta_c(r,z,0) = 0, \\ R_c(r,z,0) = 0, \quad J_v(r,0) = J_{v,0}. \end{cases} \tag{24}$$

At the initial stage, the filter is considered free of sediment, without particle accumulation, and adsorptionally unsaturated. As a result, both the cake layer thickness and the additional hydraulic resistance are taken to be zero. The initial velocity and pressure distribution is determined by solving the hydrodynamic equations stabilized under membrane non-contamination conditions. Accordingly, the velocity and pressure fields are initialized using a stationary hydrodynamic solution.

3 Solution of the problem

The mathematical model described above consists of a coupled system of flow and mass transport equations governing the filtration process in a cylindrical porous medium. Due to the nonlinear coupling between the flow variables, solute transport, adsorption, particle deposition, and changes in the porous structure, an analytical solution of the complete problem is not available. Therefore, numerical methods are employed to obtain the distributions of the pressure, velocity, concentration, and porosity.

In the present study, the problem is solved using two different numerical approaches: the Finite Difference Method (FDM) and the Finite Volume Method (FVM). To ensure an objective comparison, both methods are applied to the same mathematical model under identical physical parameters, computational domain, initial conditions, and boundary conditions. The numerical solutions are subsequently analyzed to evaluate the differences in the obtained results and to assess the accuracy and convergence characteristics of each approach.

The following subsections describe the main principles of the two numerical methods and the procedure used to compare their results.

3.1 Computational domain and grid

The filtration process is considered in an axisymmetric cylindrical porous filter. The computational domain is described in the radial and axial coordinates (r,z) as

$$0 \leqslant r \leqslant R, \; 0 \leqslant z \leqslant H,$$

where R and H denote the radius and length of the porous filter, respectively. Owing to the assumption of axisymmetry, the three-dimensional problem is reduced to a two-dimensional computational domain in the (r, z) plane.

For a consistent comparison between the Finite Difference Method and the Finite Volume Method, the same computational domain and spatial resolution are employed in both numerical approaches. The domain is discretized into N_r intervals in the radial direction and N_z intervals in the axial direction. The corresponding spatial steps are defined as

$$\Delta r = \frac{R}{N_r}, \quad \Delta z = \frac{H}{N_z}.$$

The computational nodes are defined by

$$r_i = i\Delta r, \quad i = 0, 1, \ldots, N_r,$$

and

$$z_j = j\Delta z, \quad j = 0, 1, \ldots, N_z.$$

The same spatial discretization is used as the basis for both numerical schemes in order to eliminate the influence of differences in the computational domain and grid resolution. Thus, any differences observed in the numerical results can be primarily attributed to the discretization principles of the Finite Difference and Finite Volume Methods.

For the transient filtration process, the time interval $0 \leqslant t \leqslant T$ is divided into discrete time levels,

$$t^n = n\Delta t, \quad n = 0, 1, \ldots, N_t,$$

where Δt is the time step and T is the total simulation time. The same time step is used for both numerical approaches to ensure a consistent comparison of the transient evolution of the pressure, velocity, concentration, and porosity fields.

3.2 Finite difference method

The Finite Difference Method is based on the direct approximation of the derivatives appearing in the governing equations at discrete grid points. The pressure, velocity components, concentrations, and other dependent variables are evaluated at the nodes of the computational grid defined in the (r, z) domain.

For a general variable φ, the first-order derivatives in the radial and axial directions are approximated using finite differences. The central difference approximations can be written as

$$\left(\frac{\partial \varphi}{\partial r}\right)_{i,j} \approx \frac{\varphi_{i+1,j} - \varphi_{i-1,j}}{2\Delta r},$$

and

$$\left(\frac{\partial \varphi}{\partial z}\right)_{i,j} \approx \frac{\varphi_{i,j+1} - \varphi_{i,j-1}}{2\Delta z}.$$

The corresponding second-order derivatives are approximated as

$$\left(\frac{\partial^2 \varphi}{\partial r^2}\right)_{i,j} \approx \frac{\varphi_{i+1,j} - 2\varphi_{i,j} + \varphi_{i-1,j}}{\Delta r^2},$$

and

$$\left(\frac{\partial^2 \varphi}{\partial z^2}\right)_{i,j} \approx \frac{\varphi_{i,j+1} - 2\varphi_{i,j} + \varphi_{i,j-1}}{\Delta z^2}.$$

For the convective transport terms, an upwind approximation is employed to account for the direction of the flow, while the diffusion terms are discretized using central differences. The resulting discrete equations are solved sequentially at each time level.

The pressure and velocity fields are obtained using an iterative pressure-correction procedure to satisfy the continuity equation. After determining the pressure field, the velocity components are corrected, and the transport equations are subsequently solved using the updated flow field. The adsorption, particle deposition, and porosity evolution equations are then evaluated at each time step. The time increment is selected to maintain

the numerical stability of the explicit transport calculations according to the Courant–Friedrichs–Lewy condition. Thus, the Finite Difference Method provides a node-based numerical representation of the coupled filtration process, which serves as one of the two approaches considered in the present comparative study.

3.3 Finite volume method

In the Finite Volume Method, the governing equations are solved by dividing the computational domain into a set of control volumes. Unlike the Finite Difference Method, which approximates derivatives directly at discrete grid points, the Finite Volume Method is based on the integral form of the conservation equations. This approach ensures that the balance of mass and other transported quantities is satisfied within each control volume.

For a general transport variable φ, the governing equation can be expressed as

$$\frac{\partial \varphi}{\partial t} + \nabla \cdot (\mathbf{u}\varphi) = \nabla \cdot (D \nabla \varphi) + S_\varphi,$$

where $\mathbf{u}$ is the velocity vector, D is the diffusion coefficient, and S_φ represents the corresponding source or reaction term. Integrating this equation over an arbitrary control volume V gives

$$\frac{d}{dt} \int_V \varphi \, dV + \int_{\partial V} \mathbf{u}\varphi \cdot \mathbf{n} \, dA = \int_{\partial V} D \nabla \varphi \cdot \mathbf{n} \, dA + \int_V S_\varphi \, dV.$$

where ∂V denotes the boundary of the control volume and $\mathbf{n}$ is the outward normal vector.

For the axisymmetric cylindrical geometry, the control volumes are constructed in the (r, z) plane while accounting for the variation of the volume and face areas in the radial direction. The convective and diffusive fluxes are evaluated at the faces of each control volume. The convective terms are approximated according to the local flow direction, whereas central approximations are used for the diffusive fluxes.

The pressure and velocity fields are determined using a pressure-correction procedure that enforces the continuity condition. After the flow field is obtained, the transport equations are solved using the corresponding face fluxes. The adsorption, particle deposition, and porosity evolution equations are subsequently updated at each time step.

Thus, the Finite Volume Method provides a locally conservative formulation of the coupled filtration problem. Using the same computational domain, physical parameters, initial and boundary conditions, and time step as in the Finite Difference Method allows the differences between the two approaches to be evaluated on a consistent basis.

4 Comparison of the numerical methods

To evaluate the numerical performance of the Finite Difference Method and the Finite Volume Method, both approaches are applied to the same mathematical model under identical physical and computational conditions. The comparison is based primarily on the convergence of the numerical solutions under grid refinement. This procedure makes it possible to examine how the solutions obtained by each method approach a grid-independent result as the spatial resolution is increased.

4.1 Grid convergence analysis

The accuracy of a numerical solution depends on the spatial discretization of the computational domain. Therefore, a grid convergence analysis is performed for both the Finite Difference Method and the Finite Volume Method. The computational domain

is successively refined while maintaining the same filter geometry, physical parameters, initial conditions, boundary conditions, and simulation time.

Let the characteristic grid size be denoted by h. For the two-dimensional axisymmetric domain, the grid resolution can be defined according to

$$(N_r, N_z) = \left(N_r^{(1)}, N_z^{(1)}\right), \left(N_r^{(2)}, N_z^{(2)}\right), \left(N_r^{(3)}, N_z^{(3)}\right), \ldots$$

For example, a sequence of progressively refined grids may be written as

$$25 \times 50,\ 50 \times 100,\ 100 \times 200,\ 200 \times 400.$$

The corresponding spatial steps are

$$\Delta r = \frac{R}{N_r}, \quad \Delta z = \frac{H}{N_z}.$$

For each grid, the complete numerical problem is solved independently using both methods. The resulting pressure, velocity, concentration, and porosity fields are then compared to determine the sensitivity of the solution to grid refinement.

Let φ_h denote the numerical solution obtained on a grid with characteristic size h, where φ represents any of the calculated variables, such as

$$\varphi \in \{p, u_r, u_z, c, \varepsilon\}.$$

As the grid is refined, a convergent numerical method should satisfy

$$\varphi_h \to \varphi, \quad h \to 0,$$

where φ represents the grid-independent numerical solution. In the present study, the convergence behavior of the two methods is evaluated by examining the differences between solutions obtained on successive grids.

For two consecutive grids with sizes h and $h/2$, the relative difference can be calculated as

$$E_h = \frac{\left\|\varphi_h - \varphi_{h/2}\right\|_2}{\left\|\varphi_{h/2}\right\|_2},$$

where $\|\cdot\|_2$ denotes the discrete L_2 norm. For a two-dimensional computational domain, this norm is defined as

$$\|\varphi\|_2 = \left[\sum_{i=1}^{N_r}\sum_{j=1}^{N_z} \varphi_{i,j}^2 \Delta V_{i,j}\right]^{1/2},$$

where $\Delta V_{i,j}$ is the volume associated with the corresponding computational location. In the axisymmetric geometry, the volume weighting accounts for the radial dependence of the cylindrical control region.

The maximum difference between the solutions on successive grids can also be evaluated using the L_∞ norm,

$$E_\infty = \max_{i,j} \left|\varphi_{h,i,j} - \varphi_{h/2,i,j}\right|.$$

A decreasing value of these quantities with increasing grid resolution indicates that the numerical solution is approaching a grid-independent result.

To estimate the order of convergence, three successively refined grids can be considered. Assuming a refinement ratio

$$r = \frac{h_{\text{coarse}}}{h_{\text{fine}}},$$

the observed order of convergence may be estimated as

$$p_{\text{obs}} = \frac{\ln\left(\left|\frac{\varphi_h - \varphi_{h/r}}{\varphi_{h/r} - \varphi_{h/r^2}}\right|\right)}{\ln r}.$$

For a uniform refinement in which the spatial step is reduced by a factor of two,

$$r = 2,$$

and therefore

$$p_{\text{obs}} = \frac{\ln\left(\left|\frac{\varphi_h - \varphi_{h/2}}{\varphi_{h/2} - \varphi_{h/4}}\right|\right)}{\ln 2}.$$

The grid convergence analysis is performed separately for the Finite Difference and Finite Volume methods. The calculated convergence errors and observed orders are then compared for the principal variables of the numerical model.

It should be noted that grid convergence alone does not provide the exact error unless an analytical or highly accurate reference solution is available. Nevertheless, when the solutions become insensitive to further grid refinement, the finest-grid solution can be used as a numerical reference for the subsequent quantitative accuracy analysis. The relative L_2 error and NRMSE of both methods with respect to the reference solution at different times are given in Table 1.

Here Rel. L_2 is Relative L_2 error.

The Relative L_2 error measures the overall difference between the numerical solution and the reference solution.

$$\text{Relative } L_2 = \frac{\sqrt{\sum_{i,j} \left(\varphi_{i,j} - \varphi_{i,j}^{\text{ref}}\right)^2}}{\sqrt{\sum_{i,j} \left(\varphi_{i,j}^{\text{ref}}\right)^2}} \times 100\%.$$

where φ is the solution being tested (FDM or FVM), φ^{ref} is the reference solution, and i, j are the grid indices. A smaller Relative L_2 value means the numerical result is closer to the reference solution.

For the pressure at $t = 100$ s the values are

Method	Relative L_2, %
FDM	0.1601
FVM	2.0294

Therefore, according to this measure, FDM is more accurate for p at $t = 100$ s.

NRMSE means Normalized Root Mean Square Error. First, the RMSE is calculated as

Table 1 Verification of FDM and FVM against the reference solution: relative L_2 error and NRMSE.

Time, s	Variable	FDM Rel. L_2, %	FVM Rel. L_2, %	FDM NRMSE, %	FVM NRMSE, %	Better
100	p	0.1601	0.2294	0.0276	0.3494	FDM
100	u_z	142.0945	373.9049	63.826	168.096	FDM
100	u_r	1127.3890	3041.7732	464.9247	1254.434	FDM
100	c	51.3937	122.0187	20.4090	48.4549	FDM
100	ε	0.2700	1.3089	0.2488	1.2058	FDM
500	p	0.0457	2.0026	0.0079	0.3448	FDM
500	u_z	34.1220	91.2612	15.3405	41.0291	FDM
500	u_r	259.7437	691.2568	107.1111	285.0530	FDM
500	c	11.3193	26.8159	4.4950	10.6489	FDM
500	ε	0.2764	1.3228	0.2544	1.2172	FDM
1000	p	0.0336	2.0005	0.0058	0.3444	FDM
1000	u_z	21.2223	56.2285	9.5411	25.2791	FDM
1000	u_r	149.5183	411.3822	61.6572	169.6427	FDM
1000	c	6.3901	15.2981	2.5376	6.0751	FDM
1000	ε	0.2814	1.3085	0.2587	1.2027	FDM
2000	p	0.0294	2.0014	0.0051	0.3446	FDM
2000	u_z	15.1539	41.7600	6.9053	18.7147	FDM
2000	u_r	99.1459	264.8455	40.8550	109.2187	FDM
2000	c	3.8794	9.4408	1.5406	3.7400	FDM
2000	ε	0.2851	1.3141	0.2617	1.2059	FDM

$$\mathrm{RMSE} = \sqrt{\frac{1}{N}\sum_{i,j}\left(\varphi_{i,j} - \varphi_{i,j}^{\mathrm{ref}}\right)^2}.$$

Then it is normalized. For example, if normalized by the range of the reference solution,

$$\mathrm{NRMSE} = \frac{\mathrm{RMSE}}{\varphi_{\max}^{\mathrm{ref}} - \varphi_{\min}^{\mathrm{ref}}} \times 100\%.$$

A smaller NRMSE means better agreement with the reference solution.

For the pressure:

Method	NRMSE, %
FDM	0.0276
FVM	0.3494

Thus, FDM is again closer to the reference solution. The RMSE and NRMSE values in absolute units are summarized in Table 2.

MAE means Mean Absolute Error.

$$\mathrm{MAE} = \frac{1}{N}\sum_{i=1}^{N}\left|\varphi_i - \varphi_i^{\mathrm{ref}}\right|.$$

For the two-dimensional solution,

Table 2 Verification of FDM and FVM against the reference solution: RMSE and NRMSE.

Time, s	Variable	FDM RMSE	FVM RMSE	FDM NRMSE	FVM NRMSE	Better
100	p	4.997716×10^{-3}	6.332328×10^{-2}	3.966767×10^{-3}	2.702509×10^{-2}	FDM
100	u_z	3.039235×10^{-3}	7.973990×10^{-3}	2.412872×10^{-3}	6.370256×10^{-3}	FDM
100	u_r	2.988440×10^{-3}	8.086939×10^{-3}	2.387710×10^{-3}	6.442519×10^{-3}	FDM
100	c	5.033488×10^{-3}	1.150249×10^{-2}	4.033100×10^{-3}	9.532990×10^{-3}	FDM
100	ε	9.913855×10^{-4}	4.805595×10^{-2}	7.877276×10^{-4}	4.069580×10^{-3}	FDM
500	p	4.971987×10^{-3}	2.179322×10^{-1}	3.919204×10^{-4}	7.883104×10^{-3}	FDM
500	u_z	3.017636×10^{-3}	8.070829×10^{-3}	2.407738×10^{-3}	6.412237×10^{-3}	FDM
500	u_r	3.036265×10^{-3}	8.804204×10^{-3}	2.226674×10^{-3}	6.411153×10^{-3}	FDM
500	c	5.028125×10^{-3}	1.191175×10^{-2}	3.992288×10^{-3}	9.524755×10^{-3}	FDM
500	ε	1.000607×10^{-3}	4.780018×10^{-3}	7.993324×10^{-4}	4.003784×10^{-3}	FDM
1000	p	5.004582×10^{-3}	2.978019×10^{-1}	3.983857×10^{-3}	1.049114×10^{-2}	FDM
1000	u_z	3.015186×10^{-3}	7.988712×10^{-3}	2.401960×10^{-3}	6.375095×10^{-3}	FDM
1000	u_r	3.001346×10^{-3}	8.245522×10^{-3}	2.387019×10^{-3}	6.570815×10^{-3}	FDM
1000	c	5.049133×10^{-3}	1.208709×10^{-2}	4.051030×10^{-3}	9.686012×10^{-3}	FDM
1000	ε	1.004187×10^{-3}	4.686896×10^{-3}	8.189080×10^{-4}	3.917969×10^{-3}	FDM
2000	p	4.975390×10^{-3}	3.825440×10^{-1}	3.970512×10^{-3}	1.186533×10^{-2}	FDM
2000	u_z	2.985003×10^{-3}	8.115756×10^{-3}	2.380884×10^{-3}	6.505738×10^{-3}	FDM
2000	u_r	3.010776×10^{-3}	8.042816×10^{-3}	2.404136×10^{-3}	6.398908×10^{-3}	FDM
2000	c	4.924556×10^{-3}	1.194216×10^{-2}	3.955092×10^{-3}	9.549248×10^{-3}	FDM
2000	ε	9.970235×10^{-4}	4.594210×10^{-3}	7.973561×10^{-4}	3.835241×10^{-3}	FDM

$$\mathrm{MAE} = \frac{1}{N_r N_z} \sum_{i=1}^{N_r} \sum_{j=1}^{N_z} \left| \varphi_{i,j} - \varphi_{i,j}^{\mathrm{ref}} \right| .$$

Smaller MAE means a more accurate solution. Unlike RMSE, MAE treats all errors proportionally. A larger error does not receive extra weight through squaring.

Figure 1 presents the L_2 error of the FDM and FVM methods for different grid spacings. As the grid is refined and the grid spacing decreases, the numerical error decreases for both methods, indicating convergence toward the reference solution. The FDM and FVM curves show very similar trends, with only a small difference in error, demonstrating comparable numerical accuracy and convergence behavior.

Figure 2 compares the computational efficiency of the FDM and FVM methods by showing the runtime for different numbers of grid cells. The computational time increases as the number of grid cells increases for both methods. At the smaller grid size, the FVM method requires slightly less runtime, while at the larger grid size, the FDM method is slightly faster. Overall, both methods show similar computational performance, with only small differences in runtime.

Figure 3 shows the final concentration distribution along the axial position from $z =$ $= 0.10$ to $0.15\,\mathrm{m}$. Both FDM and FVM predict a similar decrease in concentration along the filter. The FDM values are slightly higher than the FVM values, but the difference is very small. This indicates that both numerical methods provide closely matching results and comparable accuracy for the 100×100 grid.

Figure 4 shows the final concentration distribution along the axial position from $z =$ $= 0.10$ to $0.15\,\mathrm{m}$ using the 200×200 grid. Both methods predict a similar decreasing concentration trend, particularly near the end of the selected region. The FDM results remain slightly higher than the FVM results, with a small but more visible difference than

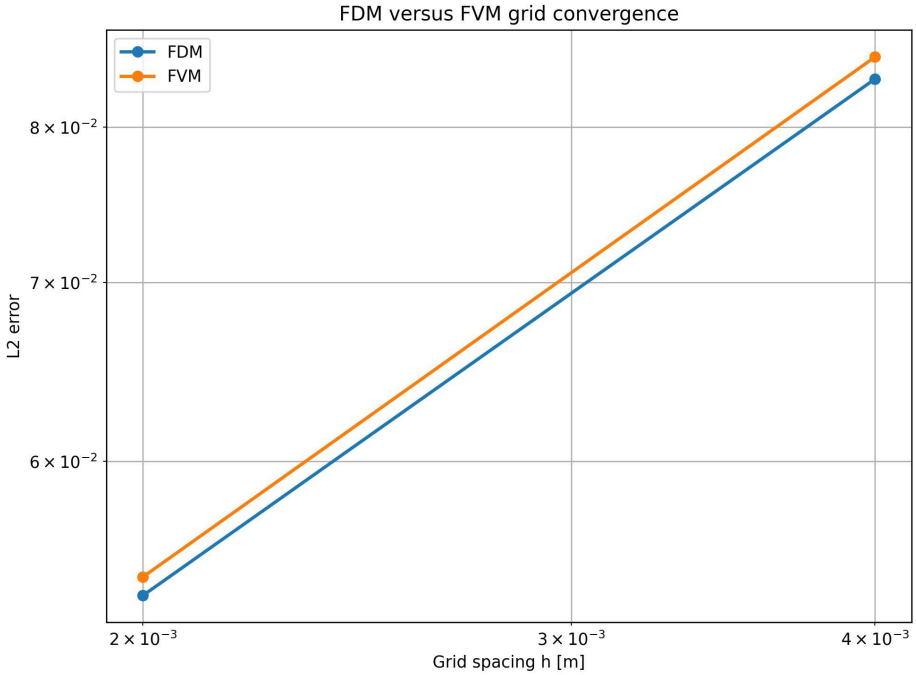

Figure 1 FDM versus FVM grid convergence.

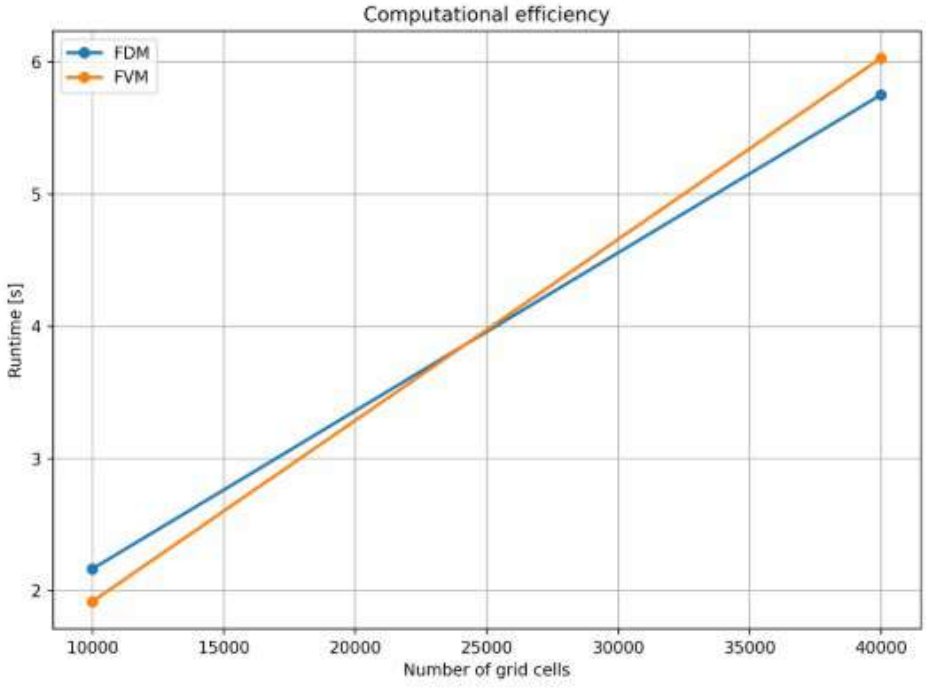

Figure 2 Computational efficiency of FDM and FVM.

in the 100×100 grid. Overall, both methods provide consistent results and demonstrate comparable numerical behavior.

5 Conclusion

This study presented a comparative numerical investigation of the Finite Difference Method (FDM) and the Finite Volume Method (FVM) for simulating filtration and

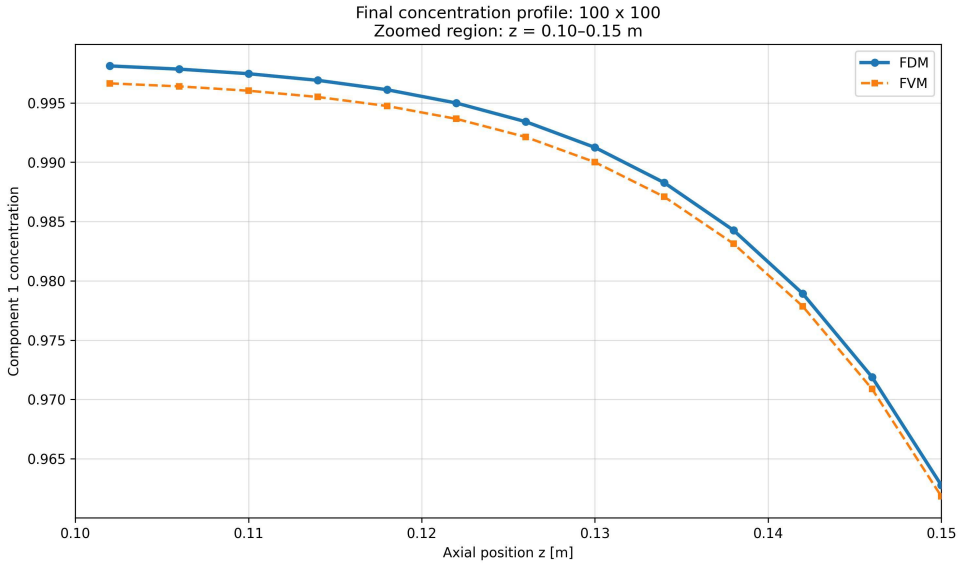

Figure 3 Final concentration profile comparison between FDM and FVM for the 100×100 grid.

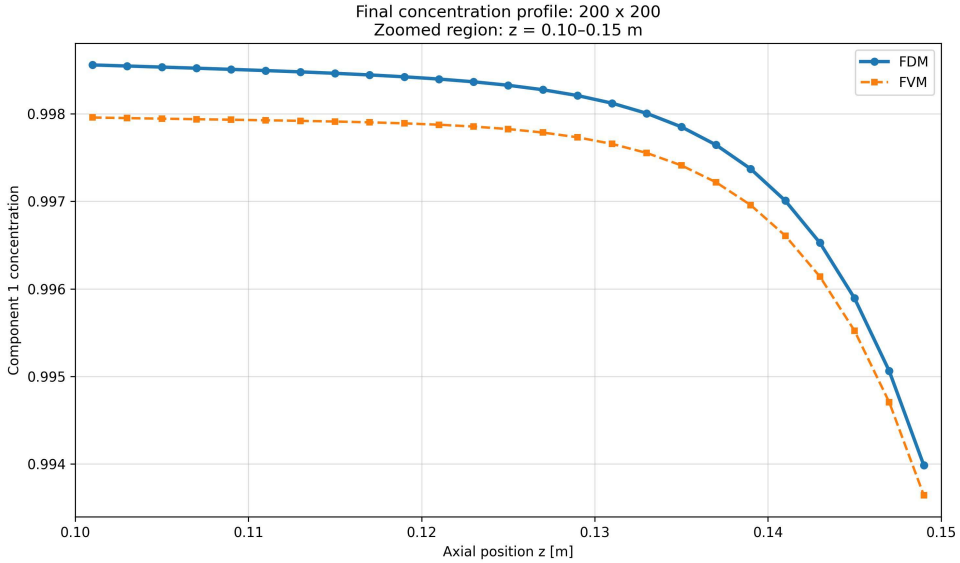

Figure 4 Final concentration profile comparison between FDM and FVM for the 200×200 grid.

mass transport processes in a cylindrical porous filter. Both methods were applied to the same axisymmetric Brinkman–Darcy flow model coupled with advection–diffusion–reaction equations under identical physical parameters, computational domains, initial conditions, and boundary conditions. The numerical model also accounts for adsorption, particle deposition, porosity variation, and changes in the permeability of the porous medium, allowing the main physical processes occurring during filtration to be represented.

The numerical results demonstrate that both FDM and FVM provide stable and convergent solutions. Grid refinement leads to a reduction in the numerical error for both methods, confirming their convergence toward the reference solution. The pressure, velocity, concentration, and porosity distributions obtained by the two approaches show generally similar behavior. The concentration profiles predicted by FDM and FVM are also in close agreement, although small differences become visible for finer computational

grids. The computational efficiency analysis further shows that both methods have comparable runtime performance, with only minor differences depending on the grid resolution. However, the quantitative error analysis based on the Relative L2 error, NRMSE, RMSE, and MAE indicates that, for the considered reference solution and simulation conditions, the FDM produced lower errors than the FVM for the investigated variables.

Overall, both numerical approaches are suitable for modeling filtration processes in cylindrical porous media. The FDM demonstrated higher accuracy for the present computational problem, while the FVM retains the important advantage of local conservation through its control-volume formulation. Therefore, the selection of the numerical method should depend on the specific objectives of the simulation, including the required accuracy, conservation properties, computational efficiency, and complexity of the filtration model. The developed comparison provides a useful basis for further studies involving more complex porous structures, nonlinear filtration conditions, and additional physical processes such as membrane fouling and long-term changes in filter properties.

Declarations

Conflicts of interest. The authors declare no conflict of interest.

Data availability. The data are available from the authors on reasonable request.

References

[1] Ravshanov N., Boborakhimov B. I., Berdiyorov Sh. Sh. 2026. Membrane fouling characteristics during filtration and transport processes in a cylindrical porous filter. *Problems of Computational and Applied Mathematics*. 3(73): 104–124. doi: https://doi.org/10.71310/pcam.3_73.2026.08.

[2] Ravshanov N., Boborakhimov B. I., Berdiyorov Sh. Sh. 2025. Numerical modeling of liquid solution filtration in a cylindrical porous filter. *Problems of Computational and Applied Mathematics*. 5(69). doi: https://doi.org/10.71310/pcam.5_69.2025.04.

[3] Ravshanov N., Boborakhimov B. I., Berdiyorov Sh. Sh. 2026. Numerical modeling of filtration and transport processes in a cylindrical porous filter using the finite volume method. *Problems of Computational and Applied Mathematics*. 1(71). doi: https://doi.org/10.71310/pcam.1_71.2026.03.

[4] Ravshanov N., Abdullaev Z., Khafizov O. 2020. Modeling the filtration of groundwater in multilayer porous media. *Construction of Unique Buildings and Structures*. 92: Art. 9206.

[5] Ravshanov N., Turakulov J., Turkmanova S., Ungalov S. 2025. Numerical study of technological process of liquid solution filtration. *AIP Conference Proceedings*. 3256: Art. 040017. doi: https://doi.org/10.1063/5.0267147.

[6] Fujisawa K., Murakami A. 2018. Numerical analysis of coupled flows in porous and fluid domains by the Darcy–Brinkman equations. *Soils and Foundations*. 58(5): 1240–1259. doi: https://doi.org/10.1016/j.sandf.2018.07.003.

[7] Wang X., Liu W., Feng Y. 2023. Modeling and numerical analysis of compressible Darcy–Brinkman fluid flow in fractured media with finite volume method on non-matching grids. *Journal of Computational and Applied Mathematics*. 420: Art. 114774. doi: https://doi.org/10.1016/j.cam.2022.114774.

[8] Ahusborde E., El Ossmani M., Id Moulay M. 2019. A fully implicit finite volume scheme for single phase flow with reactive transport in porous media. *Mathematics and Computers in Simulation*. 164: 3–23. doi: https://doi.org/10.1016/j.matcom.2018.09.001.

[9] Zhu X., Liu W. 2026. A space–time fourth-order compact finite difference scheme for semilinear compressible Darcy–Brinkman model. *Mathematical Methods in the Applied Sciences*. 49(9): 9336–9355. doi: https://doi.org/10.1002/mma.70525.

[10] Liu W., Chen Y., Wang Z., Huang J. 2023. Second-order numerical method for coupling of slightly compressible Brinkman flow with advection–diffusion system in fractured media. *Journal of Computational Physics*. 486: Art. 112120. doi: https://doi.org/10.1016/j.jcp.2023.112120.

[11] Liu W., Wang P., Fan G. 2025. A space–time second-order algorithm based on finite volume method for Brinkman flow and reactive transport model in porous media with variable fractures. *Journal of Computational and Applied Mathematics*. 462: Art. 116468. doi: https://doi.org/10.1016/j.cam.2024.116468.

[12] Nordbotten J. M. 2014. Finite volume hydromechanical simulation in porous media. *Water Resources Research*. 50(5): 4379–4390. doi: https://doi.org/10.1002/2013WR015179.

[13] Dudun A., Feng Y. 2024. Modeling fluid flow in fractured porous media: a comparative analysis between Darcy–Darcy model and Stokes–Brinkman model. *Journal of Petroleum Exploration and Production Technology*. 14: 909–926. doi: https://doi.org/10.1007/s13202-023-01743-x.

[14] Celia M. A., Bouloutas E. T., Zarba R. L. 1990. A general mass-conservative numerical solution for the unsaturated flow equation. *Water Resources Research*. 26(7): 1483–1496. doi: https://doi.org/10.1029/WR026i007p01483.

[15] Bear J., Cheng A. H.-D. 2010. *Modeling groundwater flow and contaminant transport*. Dordrecht: Springer. 834 p. doi: https://doi.org/10.1007/978-1-4020-6684-3.

УДК 519.63

СРАВНЕНИЕ МЕТОДОВ КОНЕЧНЫХ РАЗНОСТЕЙ И КОНЕЧНЫХ ОБЪЁМОВ ДЛЯ ЧИСЛЕННОГО МОДЕЛИРОВАНИЯ ФИЛЬТРАЦИИ В ЦИЛИНДРИЧЕСКОМ ПОРИСТОМ ФИЛЬТРЕ

[1*]***Бердиёров Ш.Ш.,*** [2]***Эрмонова М.У.***

*berdiyorovsh@gmail.com

[1]Научно-исследовательский институт развития цифровых технологий и искусственного интеллекта,
100125, Узбекистан, г. Ташкент, Мирзо-Улугбекский р-он, м-в Буз-2, д. 17А;
[2]Гулистанский государственный педагогический институт,
120105, Узбекистан, г. Гулистан, ул. Талабалар, 49

В данной работе представлено сравнительное численное исследование метода конечных разностей (МКР) и метода конечных объёмов (МКО) для моделирования процессов фильтрации в цилиндрическом пористом фильтре. Математическая модель сочетает в себе осесимметричные уравнения потока Бринкмана — Дарси с уравнениями адвекции — диффузии — реакции, описывающими перенос растворенных веществ в пористой среде. Оба численных метода применяются к одной и той же математической модели при идентичных начальных, граничных и вычислительных условиях. Сравнение учитывает распределение давления и скорости, концентрацию растворенного вещества, численную точность, сходимость сетки, свойства сохранения, устойчивость и вычислительную эффективность. Проведены численные

эксперименты для оценки влияния вычислительного метода на результаты моделирования. Результаты демонстрируют преимущества и различия подходов конечных разностей и конечных объемов и предоставляют основу для выбора подходящего численного метода для моделирования процессов фильтрации в цилиндрических пористых средах.

Ключевые слова: цилиндрический пористый фильтр, процессы фильтрации, модель Бринкмана — Дарси, метод конечных разностей, метод конечных объёмов, численное моделирование

Цитирование: *Бердиёров Ш.Ш., Эрмонова М.У.* Сравнение методов конечных разностей и конечных объёмов для численного моделирования фильтрации в цилиндрическом пористом фильтре // Проблемы вычислительной и прикладной математики. – 2026. – № 4(74). – С. 65-84.

DOI: 10.71310/pcam.4_74.2026.04

№ 4(74) 2026

ISSN 2181-8460

HISOBLASH VA AMALIY MATEMATIKA MUAMMOLARI

ПРОБЛЕМЫ ВЫЧИСЛИТЕЛЬНОЙ И ПРИКЛАДНОЙ МАТЕМАТИКИ

PROBLEMS OF COMPUTATIONAL AND APPLIED MATHEMATICS

AiRI
RAQAMLI TEXNOLOGIYALAR VA SUN'IY INTELLEKTNI RIVOJLANTIRISH ILMIY-TADQIQOT INSTITUTI

ПРОБЛЕМЫ ВЫЧИСЛИТЕЛЬНОЙ И ПРИКЛАДНОЙ МАТЕМАТИКИ

№ 4(74) 2026

Журнал основан в 2015 году.
Издается 6 раз в год.

Учредитель:
Научно-исследовательский институт развития цифровых технологий и искусственного интеллекта.

Журнал зарегистрирован в Агентстве информации и массовых коммуникаций при Администрации Президента Республики Узбекистан.
Свидетельство №0856 от 5 августа 2015 года.

ISSN 2181-8460, eISSN 2181-046X

Адрес редакции:
100125, г. Ташкент, м-в. Буз-2, 17А.
Тел.: +(998) 71 263-41-98.
Э-почта: journals@airi.uz.
Веб-сайт: https://journals.airi.uz.

Дизайн и вёрстка:
Шарипов Х.Д.

Отпечатано в типографии НИИ РЦТИИ.
Подписано в печать 25.08.2026 г.
Формат 60x84 1/8. Заказ № 4. Тираж 100 экз.

PROBLEMS OF COMPUTATIONAL AND APPLIED MATHEMATICS

No. 4(74) 2026

The journal was established in 2015.
6 issues are published per year.

Founder:
Digital Technologies and Artificial Intelligence Development Research Institute.

The journal is registered by Agency of Information and Mass Communications under the Administration of the President of the Republic of Uzbekistan.
Certificate of Registration No. 0856 of 5 August 2015.

ISSN 2181-8460, eISSN 2181-046X

Address:
100125, Tashkent, Buz-2, 17A.
Tel.: +(998) 71 263-41-98.
E-mail: journals@airi.uz.
Web-site: https://journals.airi.uz.

Layout design:
Sharipov Kh.D.

DTAIRI printing office.
Signed for print 25.08.2026
Format 60x84 1/8. Order No. 4. Print run of 100 copies.

Содержание

Contents